Süleyman Demirel Üniversitesi Fen Edebiyat Fakültesi Fen Dergisi
Süleyman Demirel University Faculty of Arts and Sciences Journal of Science
2018, 13(2): 108-120
DOI: 10.29233/sdufeffd.466722

X-Ray and Theoretical Studies of 4-((4-(tert-butyl)benzylidene)amino)-1,5-dimethyl-2-phenyl-1,2-dihydro-*3H*-pyrazol-3-one

Şehriman ATALAY[*1]

[*1] *Ondokuz Mayıs University, Science and Arts Faculty, Department of Physics, 55139, Samsun, Turkey*
**corresponding author e-mail: atalays@omu.edu.tr*

(Received: 02.10.2018, Accepted: 05.11.2018, Published: 30.11.2018)

Abstract: The molecular structure of [4-((4-(tert-butyl)benzylidene)amino)-1,5-dimethyl-2-phenyl-1,2-dihydro-3H-pyrazol-3-one crystal and some physical and chemical properties were investigated using single crystal X-ray diffraction, FT-IR, UV and quantum mechanical methods. The compound studied in this study is the Schiff base compound and crystalizes in monoclinic space group I2/a. The molecule is not planar. The crystal structure is stabilized by intermolecular C-H…..π interactions. Theoretically, it was investigated using Density Functional Theory (DFT) and Hartree-Fock Roothann Method compared with the experimental results and it was seen that both results were in agreement with each other. In the DFT and HF calculations, the B3LYP / 6-31G +d base set and Berny's method were used.

***Key words**:* Schiff base compounds, DFT and HF calculations, X-ray Diffractions, FT-IR, and UV-vis spectrums.

4 - ((4- (tert-bütil) benziliden) amino)-1,5-dimetil-2-fenil-1,2-dihidro-3H-pirazol-3-on'un X-ışını ve Teorik Çalışmaları

Özet:[4-((4-(tert-bütil) benziliden) amino)-1,5-dimetil-2-fenil-1,2-dihidro-3H-pirazol-3-on kristalinin moleküler yapısı ve bazı fiziksel ve kimyasal özellikleri tek kristal X-ışını kırınımı, FT-IR, UV ve kuantum mekaniksel yöntemleri kullanılarak araştırıldı. Bu çalışmada incelenen bileşik Schiff bazı bileşiktir ve bileşik monoklinik kristal sisteminde kristalleşmiştir, uzay grubu ise I2/ a'dır. Molekül düzlemsel değildir. Kristal yapı moleküller arası C-H…π etkileşimleri ile stabilize edilmiştir. Teorik olarak, Yoğunluk Fonksiyonel Kuramı (YFK) ve Hartree-Fock Roothann (HF) yöntemi kullanılarak araştırılmış ve deneysel sonuçları ile karşılaştırılması yapılmıştır. Yapılan hesaplamalar sonucunda bu iki teorik hesaplama sonucunun deneysel sonuçlar ile örtüştüğü gözlendi. YFK ve HF yöntemi hesaplamalarında B3LYP / 6-31G +d baz seti ve Berny yöntemi kullanıldı.

***Anahtar kelimeler**:* Schiff bazı bileşikleri, YFK ve HF hesaplamaları, X-ışını Difraksiyonları, FT-IR ve UV-vis spektrumları.

1. Introduction

In single crystals, molecules form a regular structure. Physicists and chemists must write the Hamilton equation to solve the crystal structure and solve the Schrodinger equation. The analytical solution of the Schrödinger equation for multi-electron systems is nowadays impossible due to the mathematical solution. Therefore, theoretically, approximate methods and different experimental methods are used for structure analysis. The most effective method used theoretically is the 'Hartree-Fock Roothann Method' while the experimental most effective method is the X-ray method.

For Citation: Ş. Atalay, "X-Ray and Theoretical Studies of 4-((4-(tert-butyl)benzylidene)amino)-1,5-dimethyl-2-phenyl-1,2-dihydro-3H-pyrazol-3-one", *Süleyman Demirel Üniversitesi Fen Edebiyat Fakültesi Fen Dergisi*, 13(2), 108-120, 2018.

When atoms are bonding to form any molecule, they do not behave randomly, they become selective. They are connected using rules in the formation of nature. As a result of this analysis, we solve the structures by using the spectroscopic methods presented by technology. The best experimental method we know now is X-ray diffraction method.

As a result of the analysis made by X-ray diffraction method, a common nomenclature was made for some molecular structures according to the chemical bonds formed between atoms. Schiff bases, one of these important groups, have important applications in many different areas. The use of Schiff bases which are obtained from the condensation of primary amines and effective carbonyl groups has caused to an increment in their syntheses and consideration of their biological effectiveness in both the pharmaceutical and industrial areas [1]. Schiff bases which have a double C=N bond behave as a chelating ligands with different transition metals by coordinating to give complex compounds. Schiff bases and their metal complexes have significant duties in living systems [2]. The some of their remarkable biological performances are such as antipyretic, anti-proliferative, antiviral, antibacterial, anticancer, anti-inflammatory, antimalarial, antifungal and oxygen carrier features [3]. In addition to biological activities Schiff bases have miscellaneous utilizations in organic supplies (as the corrosion inhibitor and polymers), analytical (as the analytical products) and inorganic chemistry (as the catalysts) [4], optoelectronic technology (for design of various molecular electronic devices) [5] and industrial areas (as the pigments, dyes and also fluorescent sensors for toxic metal ions) [6]. Besides, in recent years especially 4-aminoantipyrine based Schiff bases and their complexes have very popular area in bioengineering, molecular biology and antineoplastic medication [7,8].

In this work, the molecular structure of [4-((4-(tert-butyl)benzylidene)amino)-1,5-dimethyl-2-phenyl-1,2-dihydro-3H-pyrazol-3-one [$C_{22}H_{25}N_3O$] crystal and some physical and chemical properties were investigated using single-crystal X-ray diffraction, FT-IR, UV and quantum mechanical methods. Theoretically and experimentally found the most stable geometric structures, bond lengths, bond angles and torsion angles are given comparatively. In addition, using DFT, HF, molecular electrostatic potential surface and boundary orbitals were obtained.

2. Material and Method

The chemicals and solvents were supplied by Sigma and Merck without more purification. Melting point was determined in open glass capillaries on Electrothermal IA9200 melting point apparatus and are uncorrected. The FTIR spectrum in the range (600-4000) cm^{-1} at a resolution of 8 cm^{-1} was recorded with Attenuated Total Reflection (ATR) technique on Shimadzu IRAffinity-1 FT-IR spectrometer. ^1H NMR spectrum were recorded on a Varian Mercury-400, 400 MHz while ^{13}C NMR spectra on Varian Mercury-400, 100 MHz in DMSO-d_6 as a solvent. Chemical shifts (δ) are reported in ppm and were adjusted relative to the residual solvent peak. The UV-vis absorption spectrum of the compounds was obtained in DMSO solutions ($c= 5.06 \times 10^{-4}$ mol L^{-1}): at room temperature in the range 200-900 nm with a Shimadzu UV-1800 UV-vis Spectrophotometer at a wavelength of maximum absorption (λ_{max}, nm). Elemental analysis (C, H, N) was obtained by using Elemental Vario Micro Cube, CHNS analyzer.

The formation of the organic chemical compound in this study, the synthesis of the organic crystals formed in the chemistry laboratory and experimentally obtaining the ground state structure geometry by the single crystal X-ray diffraction method, FT-IR, and UV-vis spectra of the molecule. In the next section, the experimental and theoretical results obtained by these methods are compared and interpretations.

3. Results

3.1 Synthesis

5 ml absolute methanol solution of 4-amino-1,5-dimethyl-2-phenyl-1,2-dihydro-3*H*-pyrazol-3-one ($C_{11}H_{13}N_3O$) (0.203 g/ 1 mmol) was added to 5 ml absolute methanol solution of 4-tert-butylbenzaldehyde ($C_{11}H_{14}O$) (0.162 g /1 mmol) in the presence of 1 drops of acetic acid as a catalyst. This mixture was refluxed for 2 h. The resulting solution was brought to thermal equilibrium at room temperature. The white solid of $C_{22}H_{25}N_3O$ was formed which was filtered and recrystallized in toluene (see Figure 1). Yield; 92%: m.p: 430-431 K.

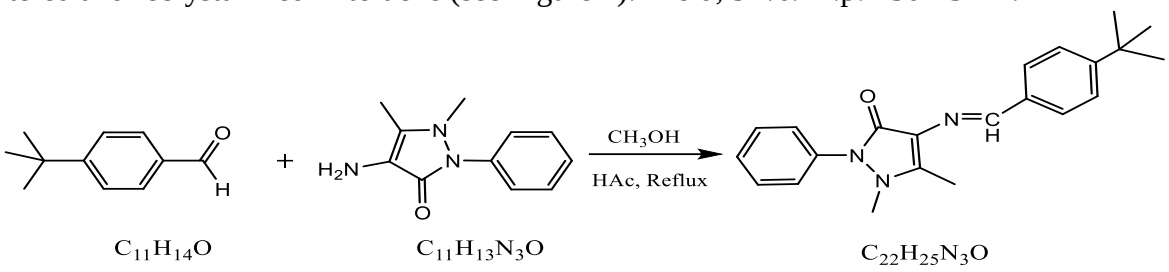

Figure 1. Synhesis reaction of $C_{22}H_{25}N_3O$

3.2 X-ray Difraction Study

In order to be suitable for crystallographic studies, a single crystal was chosen as a colourless prism. Diffraction measurements were performed on a STOE IPDS2 at room temperature (296 K) using graphite monochrome MoKa (λ = 0.71073Å) radiation in single crystal diffractometer [9].

The intensity symmetries of the space group was obtained as monoclinic I2 / a. Reflections and cell parameters were determined in the rotation mode and by the X-AREA software, respectively, [9]. The X-RED software and the integration method were used to find the an absorption correction [9].

The crystal structure was solved using direct methods in the SHELXS-97 software [10,11]. All atomic parameters without hydrogen atoms were anisotropically refined. And then, all H atom parameters were geometrically positioned and refined using a riding model with C-H = 0.93 and 0.96 A (for methyl) and U_{iso} = 1.5 U_{eq} (C). Crystallographic data and structure treatment parameters for $C_{22}H_{25}N_3O$ crystals are given in Table 1.
The molecular structure has two phenyl rings and pyrazol ring. The phenyl rings (ring1: C6-C10 and ring3: C17-C22) and pyrazol ring (ring2: N2, N3, C12, c13, C14) on the molecule have not planar conformation. The dihedral angels between these rings, 1-2, 1-3, and 2-3 are 16.00(1), 38.68(1) and 41.97(2); respectively.

The new crystal structure obtained forms a stable structure with intermolecular C-H … π interactions and the formation of this structure is shown in Figure 2. As seen from the figure, the interactions of C-H N π are between the ring (Cg 1) and the H 16B atom of the adjacent molecule [Cg 1: N 1 / N 3 / C 13 / C 12 / C 14; H16B ... cg2: 3,530 (4) Å; the symmetry code are (i) [1/2 + x, -y, z] and ring (Cg2) and H15A atom of the adjacent molecule [Cg2: C5-C10; H15A ... cg2: 3,693 (4) Å; symmetry code (i) [1 + x, y, z], respectively.

Table 1. The Table Shows Following Details for $C_{22}H_{25}N_3O$ Crystallographic data and structure refinement parameters.

Empirical formula	$C_{22}H_{25}N_3O$
Formula weight (g/mol)	347.45
Crystal system, space group	Monoclinic, I 2/a
a, b, c (Å)	7.6695(6), 18.9917(19), 29.092(2)
β(°)	94.328(5)
V(Å^3)	4225.3(6)
Z	8
Density$_{calc.}$ (g/cm^3)	1.092
Absorption coefficient(mm^{-1})	0.068
F(000)	1488
Crstal size (mm)	0.690x0.420x0.110
Reflection collected/independent	4395/1871
Parameters	240
Goodness-of-fit on F^2	0.829
Final R indices [I > 2\s(I)]	R_1= 0.050, wR_2=0.100
R indices (all data)	R_1= 0.143, wR_2=0.124
Programs	ORTEP-3[12], WinGX [12]
CCDC	1861385

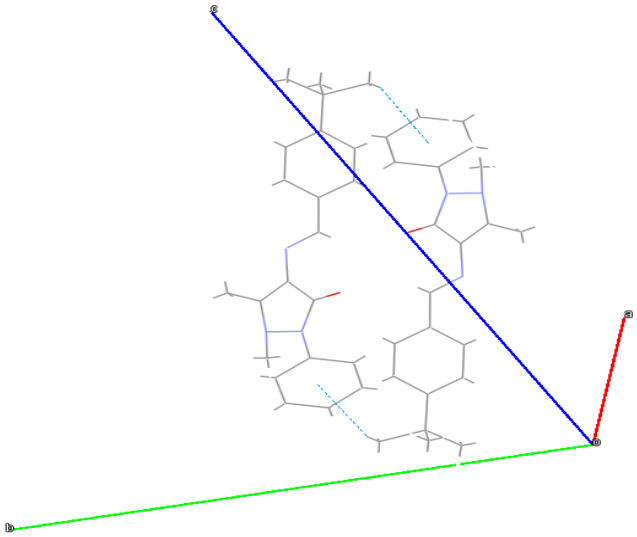

Figure 2 Diagram is shown of a stable structure C-H… π interactive structure. The dashed lines in the figure showed intermolecular C-H…π interactions.

3.3 Theoretical study

In the theoretical calculations for the $C_{22}H_{25}N_3O$ crystal, the DFT theory was chosen as the computational method and the Gaussian 03W software package [13] and the Gauss-view visualisation programme [14] was used. In these calculations, Becke's exchange function and the B3YLYP function, which is a three-parameter hybrid exchange correlation function including Lee, Yang, and Parr's terms, are used [15,16]. In order to perform the molecular modelling of $C_{22}H_{25}N_3O$, first, the coordinates of the atoms forming the molecule were obtained experimentally by the X-ray diffraction method and then the calculated vibration frequencies of the optimized molecular structure are listed in Table 2. The geometry of the optimized molecular structure of the structure obtained by X-ray diffraction method is calculated using the ORTEP-3 diagram and Gaussian software and is shown in Figure 3.

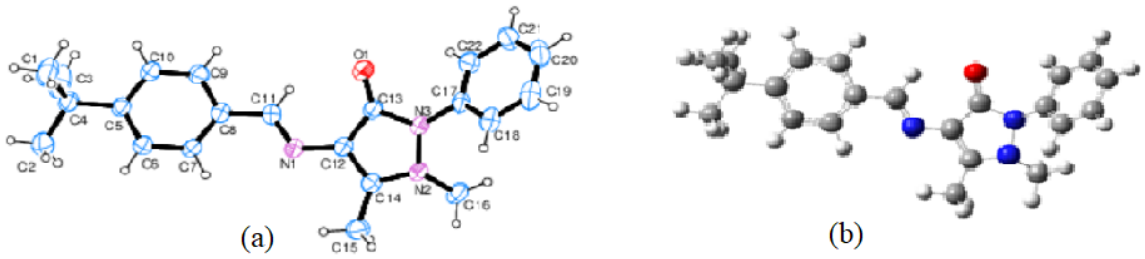

Figure 3. a) The geometry ORTEP of molecular structure obtained by X-rays can be seen. b) The optimum shape of the structure by calculated with Gaussian software.

Table 2. Geometric parameters (Å, º)

Bond Lengths	Experimental	DFT(B3LYP)	HF
O1-C13	1.231 (3)	1.2291	1.2031
N2-C14	1.369 (3)	1.3883	1.3894
N2-N3	1.409 (2)	1.4135	1.4024
N2-C16	1.475 (3)	1.469	1.4599
N3-C13	1.393 (3)	1.4158	1.383
N3-C17	1.423 (3)	1.4221	1.4218
N1-C11	1.277 (3)	1.2911	1.2622
N1-C12	1.395 (3)	1.3841	1.3899
C12-C14	1.366 (3)	1.3735	1.3428
C12-C13	1.439 (3)	1.4685	1.4681
C17-C22	1.377 (3)	1.4016	1.3882
C17-C18	1.383 (3)	1.4021	1.3884
C14-C15	1.489 (3)	1.492	1.4937
C8-C7	1.377 (3)	1.4042	1.3901
C8-C9	1.385 (3)	1.4058	1.3913
C8-C11	1.464 (3)	1.466	1.476
C5-C10	1.380 (3)	1.4067	1.3952
C5-C6	1.392 (3)	1.4071	1.3959
C5-C4	1.523 (3)	1.5395	1.5381
C9-C10	1.378 (3)	1.3926	1.3842
C22-C21	1.375 (3)	1.3955	1.3856
C7-C6	1.386 (3)	1.3935	1.3852
C4-C2	1.507 (4)	1.5415	1.5364
C4-C1	1.511 (4)	1.5485	1.5416
C4-C3	1.544 (4)	1.5486	1.5416
C18-C19	1.388 (4)	1.3965	1.3875
C20-C21	1.363 (4)	1.3982	1.3877
C20-C19	1.376 (4)	1.3973	1.3862
Bond Angles	**Experimental**	**DFT(B3LYP)**	**HF**
C14-N2-N3	106.14 (17)	106.6041	105.6357
C14-N2-C16	121.20 (19)	119.2244	117.1959
N3-N2-C16	115.68 (18)	114.2012	112.2839
C13-N3-N2	109.91 (18)	109.7356	110.2293
C13-N3-C17	125.57 (19)	123.8666	122.6976
N2-N3-C17	120.62 (18)	118.936	118.2452
C11-N1-C12	119.1 (2)	120.9763	121.4331
C14-C12-N1	123.5 (2)	123.2319	123.8494

C14-C12-C13	107.9 (2)	107.5698	107.0547
N1-C12-C13	128.3 (2)	129.1553	129.0365
C22-C17-C18	121.5 (2)	120.1378	120.1592
C22-C17-N3	117.5 (2)	118.8334	118.8853
C18-C17-N3	121.0 (2)	121.0275	120.9554
C12-C14-N2	110.6 (2)	110.8461	111.4679
C12-C14-C15	128.4 (2)	127.8261	128.1177
N2-C14-C15	121.0 (2)	121.3247	120.4132
C7-C8-C9	117.2 (2)	117.882	118.0501
C7-C8-C11	122.8 (2)	122.8706	122.7057
C9-C8-C11	120.0 (2)	119.2474	119.2442
O1-C13-N3	124.2 (2)	124.319	124.7897
O1-C13-C12	130.8 (2)	130.8295	130.0818
N3-C13-C12	104.93 (19)	104.824	105.1157
N1-C11-C8	122.7 (2)	121.9347	121.9365
C10-C5-C6	116.6 (2)	116.9995	116.9954
C10-C5-C4	119.8 (2)	120.0452	120.021
C6-C5-C4	123.6 (2)	122.9553	122.9836
C10-C9-C8	121.9 (2)	120.9734	120.9753
C21-C22-C17	118.8 (3)	119.5169	119.6936
C9-C10-C5	121.4 (2)	121.5915	121.5193
C8-C7-C6	120.9 (2)	120.8141	120.7725
C7-C6-C5	121.9 (2)	121.7395	121.6874
C2-C4-C3	107.2 (3)	108.0747	107.9053
C1-C4-C3	107.2 (3)	109.2528	109.3795
C5-C4-C3	109.8 (2)	109.4348	109.5707
C17-C18-C19	118.2 (3)	119.7209	119.7177
C21-C20-C19	119.9 (3)	119.4862	119.5045
C20-C19-C18	120.6 (3)	120.4407	120.4174
C20-C21-C22	121.0 (3)	120.6851	120.4985
C2-C4-C1	110.6 (3)	108.0504	107.9012
C2-C4-C5	112.4 (2)	112.4689	112.4436
C1-C4-C5	109.5 (2)	109.4993	109.5792
Torsion Angles	**Experimental**	**DFT(B3LYP)**	**HF**
C14-N2-N3-C13	7.1 (2)	6.7476	7.303
C16-N2-N3-C13	144.6 (2)	140.5828	136.176
C14-N2-N3-C17	166.0 (2)	157.7719	155.6783
C16-N2-N3-C17	−56.5 (3)	-68.3929	-75.4486
C11-N1-C12-C14	−164.9 (2)	-178.2582	-179.4746
C11-N1-C12-C13	21.8 (4)	4.436	3.7009
C13-N3-C17-C22	−52.8 (3)	-56.799	-64.6311
N2-N3-C17-C22	151.7 (2)	156.51	151.1476
C13-N3-C17-C18	126.3 (3)	122.7838	115.4263
N2-N3-C17-C18	−29.2 (3)	-23.9072	-28.7949
N1-C12-C14-N2	−173.2 (2)	-175.2609	-175.9227
C13-C12-C14-N2	1.3 (3)	2.548	1.4977
N1-C12-C14-C15	5.8 (4)	5.3727	3.6738
C13-C12-C14-C15	−179.7 (2)	-176.8184	-178.9058
N3-N2-C14-C12	−5.0 (3)	-5.7118	-5.3426
C16-N2-C14-C12	−139.7 (2)	-136.7826	-131.2532

N3-N2-C14-C15	175.9 (2)	173.7023	175.0255
C16-N2-C14-C15	41.2 (3)	42.6315	49.1149
N2-N3-C13-O1	170.5 (2)	173.1274	172.4307
C17-N3-C13-O1	12.8 (4)	23.8305	25.7223
N2-N3-C13-C12	−6.2 (3)	-5.1475	-6.3781
C17-N3-C13-C12	−163.9 (2)	-154.4444	-153.0865
C14-C12-C13-O1	−173.3 (3)	-176.4885	-175.7224
N1-C12-C13-O1	0.8 (5)	1.1478	1.5193
C14-C12-C13-N3	3.1 (3)	1.6284	2.999
N1-C12-C13-N3	177.2 (2)	179.2648	-179.7593
C12-N1-C11-C8	−177.8 (2)	179.9794	179.915
C7-C8-C11-N1	−2.7 (4)	-0.0335	-0.3508
C9-C8-C11-N1	176.6 (2)	-179.9952	179.6444
C7-C8-C9-C10	1.0 (4)	-0.086	-0.0086
C11-C8-C9-C10	−178.3 (2)	179.8776	179.996
C18-C17-C22-C21	−1.3 (4)	-0.2562	-0.5537
N3-C17-C22-C21	177.8 (2)	179.3304	179.5033
C8-C9-C10-C5	−1.6 (4)	-0.0062	-0.0017
C6-C5-C10-C9	0.6 (4)	0.0845	0.0014
C4-C5-C10-C9	−180.0 (2)	-179.8605	179.9984
C9-C8-C7-C6	0.4 (4)	0.0985	0.0193
C11-C8-C7-C6	179.7 (2)	-179.8636	-179.9854
C8-C7-C6-C5	−1.4 (4)	-0.0198	-0.0203
C10-C5-C6-C7	0.8 (4)	-0.0717	0.0095
C4-C5-C6-C7	−178.5 (2)	179.8716	-179.9874
C10-C5-C4-C2	172.1 (3)	-179.8244	-179.9742
C6-C5-C4-C2	−8.5 (4)	0.234	0.0226
C10-C5-C4-C1	−64.5 (3)	-59.6815	-59.9814
C6-C5-C4-C1	114.8 (3)	120.3769	120.0154
C10-C5-C4-C3	52.9 (3)	60.046	60.0336
C6-C5-C4-C3	−127.8 (3)	-119.8956	-119.9697
C22-C17-C18-C19	−0.2 (3)	-0.7456	-0.3273
N3-C17-C18-C19	−179.3 (2)	179.677	179.6144
C21-C20-C19-C18	−0.8 (4)	-0.2926	-0.3583
C17-C18-C19-C20	1.3 (4)	1.0225	0.7863
C19-C20-C21-C22	−0.8 (4)	-0.7251	-0.5334
C17-C22-C21-C20	1.9 (4)	0.9965	0.9879

In addition to the molecular structure obtained from the optimized geometry of the molecule, molecular electrostatic potential (MEP) which plays an important role in the interactions and reactions between molecules was calculated by using Gaussian software [17]. MEP is a parameter related to the electronic density of a material containing electrical charge and is very important in understanding the regions and hydrogen bonding interactions used for electrophilic and nucleophilic reactions [18-20].

One of the best ways to confirm the coordinates of the atoms that make up the molecule that is the result of DFT and HF calculation is to superposition of geometries obtained from X-ray diffraction with theoretically obtained geometry. This overlap is illustrated in Figure 4. As can be seen from Figure 4, the structures drawn by HF and DFT are in harmony with the x-ray geometry. It is the HF method that best fits with X-rays. The theoretical calculations and the

experimental data overlapped with the experimental data in Fig. 4 compared to the experimental DFT and RMSE values for experimental HF were obtained as 0.01942 and 0.01583 respectively and the bond lengths were found to be better than the HF method. When the bond angles were examined, the RMSE value for experimental DFT was found to be 0.97, RMSE values for experimental HF were obtained as 1.3431 and DFT was found to have better results for bond angles.

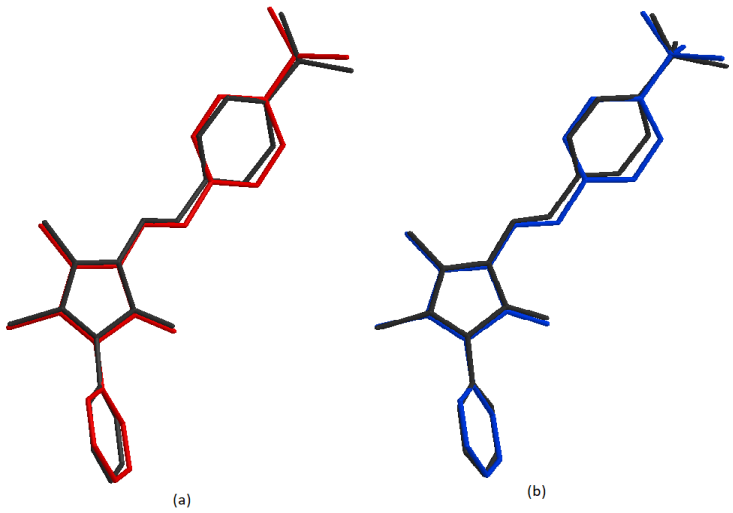

Figure 4. The molecular structure of superposition of the molecular structures calculated by DFT, HF, and X-ray structure, respectively, (red and (a), (blue and (b), and (black)).

Different values of electrostatic potentials on the surface of a molecule are typically represented by different colours; negative regions, coloured in red, denote electrophilic reactivity, while positive regions, coloured in blue, denote nucleophilic reactivity. MEP of $C_{22}H_{25}N_3O$ was calculated using the base set with the B3LYP/6-31G+d.

In the examined molecule, the negative and positive charge regions were localized at a O1with a minimum value of -0.0593 a.u and at a maximum around groups CH_3 with a maximum value of 0.0321 a.u, respectively. Positive and negative regions are associated with hydrogen bonding donor and acceptor sites. The MEP surface is shown in Figure 5.

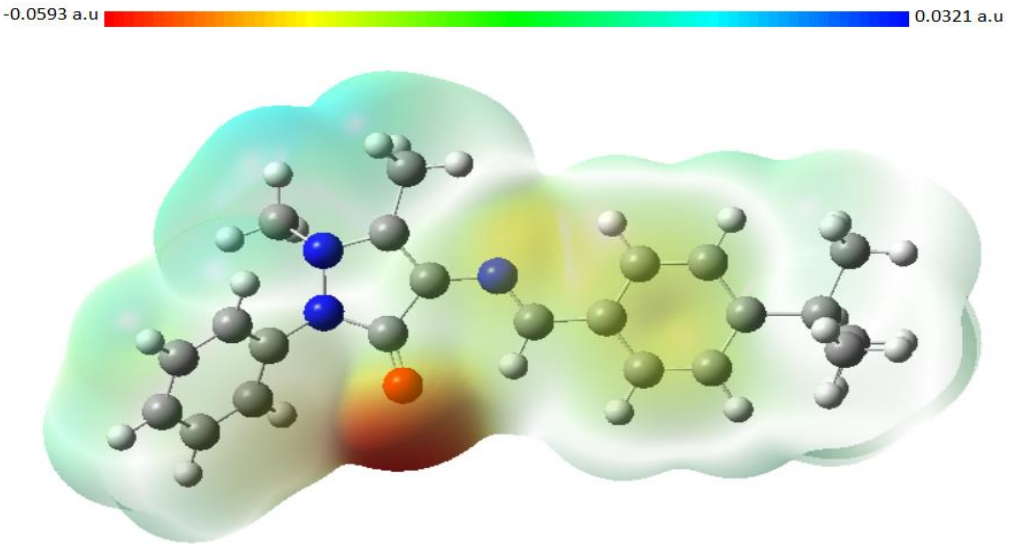

Figure 5. MEP of diagram for $C_{22}H_{25}N_3O$.

3.4. The UV-vis Spectroscopic Treatment of Title Molecule

For the examined molecule, the UV-vis spectra of the experimental absorption spectrum, in which the bands absorbed at 234 and 340 nm in DMSO are recorded, are shown in Figure 6. According to the absorption spectrum obtained, the $C_{22}H_{25}N_3O$ molecule, the density absorption wavelengths at 234 nm can be assigned to n→ n* transitions for the compound $C_{22}H_{25}N_3O$ As is known, the characteristic bands for molecular systems containing phenyl rings are in these bands. At the same time, the absorption bands at 340 nm are due to the electronic transition of n→ n*. This transition can be indicated as the groups -C=X (X: O, N).

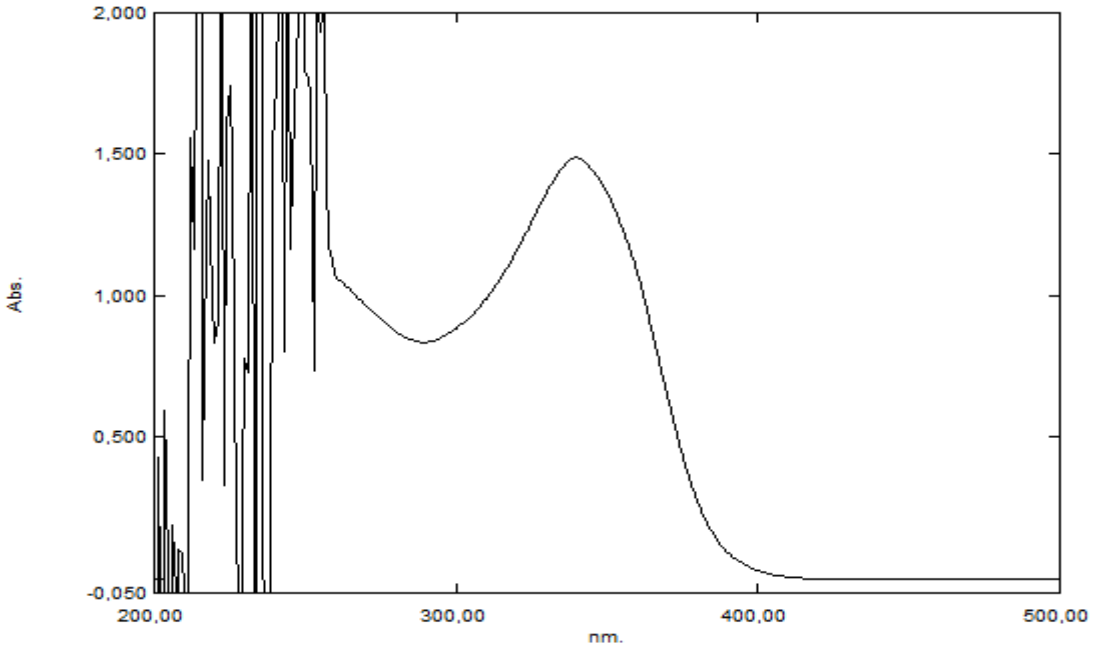

Figure 6. UV-vis spectrum in DMSO (concentration; c = 5.06 x 10^{-4}mol L^{-1}) of the compounds $C_{22}H_{25}N_3O$.

3.5. Vibrational spectrum

The characteristic vibration bands observed in the FTIR spectrum of the chemical compound studied in this study are shown in Figure 7. For the $C_{22}H_{25}N_3O$ molecule, the CH aromatic stretching modes per unit length were calculated in the range 3090.3-3052.4 cm^{-1} and this mode was observed in the interval 3074-3032 cm^{-1}. The vibrations in the $C_{22}H_{25}N_3O$ molecule were observed experimentally and some physical and chemical results obtained by calculating the theoretical conditions by using the theoretical methods of DFT and HF are given in Table 2. As seen from Table 2, the aliphatic CH stretching vibrations were observed at interval 2951-2866 cm^{-1} and calculated in the range of 2980.3-2915.5 cm^{-1}. The band attributed to the C=N stretching vibration at 1647 cm^{-1} was calculated as 1606.9 cm^{-1} for $C_{22}H_{25}N_3O$**.** The peak belonging to the carbonyl (C=O) stretching vibrations as calculated/observed are in the range of 1743 cm^{-1}/1670.9 cm^{-1} for this compound. The differences obtained for C=O/C=N vibrations are 73/41 cm^{-1} for $C_{22}H_{25}N_3O$**.** These IR spectrum results are consistent with the literature [21,22].

Tablo 3. For the $C_{22}H_{25}N_3O$ molecule, selected experimental and calculated vibration frequency values per unit length are shown. Values are given in cm^{-1}.

Vibrations	Experimental	DFT	HF
ν (C-H) Ar	3074-3032	3090.3-3052.4	3046.3-2994
ν (C-H) Alph	2951-2866	2980.3-2915.5	2974.5-2855.3
ν (C=O)	1743	1670.7	1710.5
ν (C=N)	1647	1606.9	1677.9
ν (C=C) Pyrazolone	1593	1590.9	1632.8
ν (C=C) Ar	1492-1458	1495.2-1438.6	1488-1443.6
γ (C-H) tert-butyl	1373-1230	1371.1-1244.7	1386.8-1260.1
γ (C-H) Benzene	1107-1022	1076-1059.9	1189.4-1152.6
ω (C-H)	879	881.9	847.8

(*ν*, stretching; *γ*, rocking; *ω*, wagging)

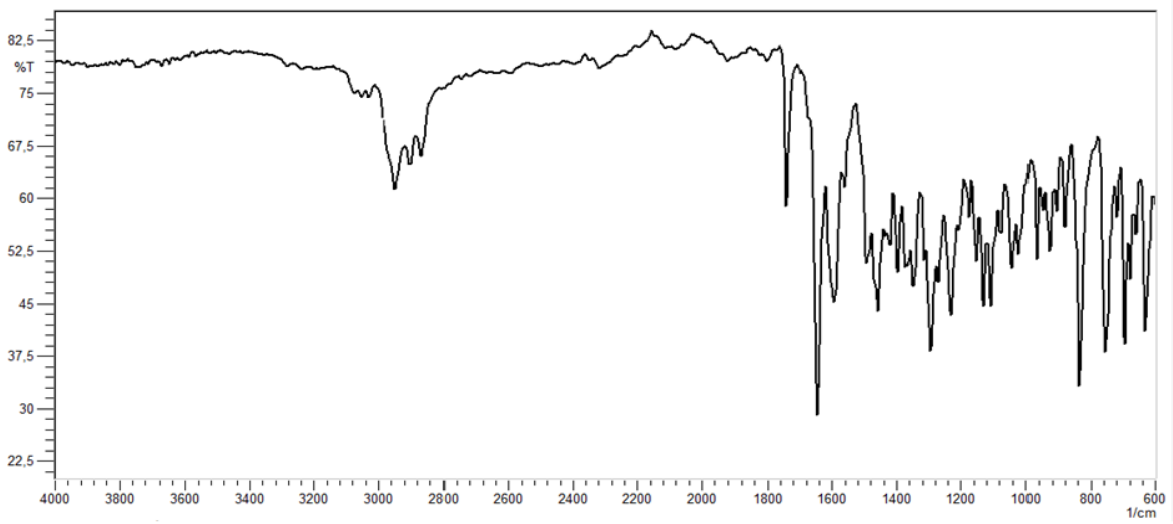

Figure 7. FTIR spectrum of the compounds $C_{22}H_{25}N_3O$

IR (ATR, *ν* cm^{-1}): 3074, 3032(Ar-CH), 2951, 2866 (Alf.-CH), 1743 (C=O), 1647 (C=N), 1593 (C=N (pyrazolone)), 1492, 1458 (Ar-C=C), 1373-1230 (*tert*-butyl CH), 1107, 1022, 879 (*p*-substituted benzene).

3.6. NMR spectra

In Figures 8 and 9, the spectroscopic characterization of the compound $C_{22}H_{25}N_3O$ is shown by ^1H and ^{13}C NMR spectroscopy. In the ^1H NMR spectrum in Figure 8, the disappearance of the amine and aldehyde groups is peaked and the presence of imines and (C11) methyl group peaks are observed in the presence of $C_{22}H_{25}N_3O$ compounds. The singlet at 9.57 ppm belonged to the N = CH proton and the phenyl proton signals appeared in pairs in DMSO-d_6 at 7.74 and at 7.49 ppm for the chemical compound examined.

The singlet assigned to N-CH_3 group, which were experimentally observed and calculated theoretically, were obtained as 3.13 and 3.49 ppm, respectively. The singlet assigned to pyrazolone ring -CH_3 group was spectroscopically determined at 2.46 ppm and theoretically

calculated at 2.42 ppm. The *tert*-Butyl protons resonated experimentally at 1.31 ppm singlet that was numerically using software in the range of 1.33 ppm.

As can be seen from the ^{13}C NMR spectrum in Figure 9, the total number of carbon peaks was well matched to the composition of compound I and the ^{13}C NMR spectrum confirmed the formation of the compound examined. The peak at 160.06 ppm belongs to HC=N group (C11) was calculated as 163.70 ppm. Chemical shift value of the carbon (C13) atom in the carbonyl group (C=O) which binds to the pyrozolone ring for $C_{22}H_{25}N_3O$ calculated chemical shift values were calculated as 160.70 ppm, respectively, were recorded at 154.83 ppm. As can be seen from Figure 9, the peaks obtained at 35.88, 35.07, 31.46 and 10.24 ppm respectively belong to N-CH3, tert-Bu-C, tert-These CH3 groups and to the pyrazolone ring -CH3. These groups were calculated as 34.9, 31.3, 31.3 and 13.0 ppm. The results of these NMR spectra are consistent with the literature [23].

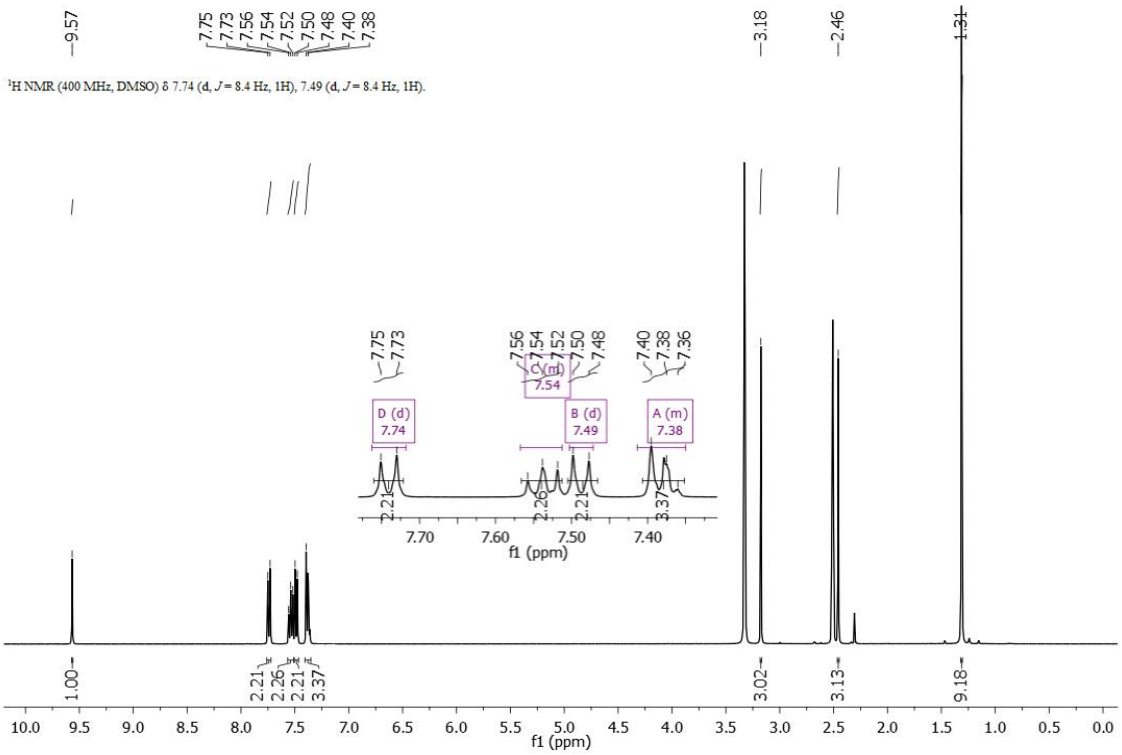

Figure 8. Experimental ^1H NMR spectra in DMSO-d_6 of the compound $C_{22}H_{25}N_3O$.

^{1}H NMR (DMSO-d_6, 400 MHz, δ ,ppm):9.57 (s, 1H, -CH=N-), 7.74 (d, 2H, *J*=8.4 Hz Ph), 7.54 (m, 2H, PyrazolonePh), 7.49 (d, 2H, *J*=8.4 Hz Ph), 7.38 (m, 3H, PyrazolonePh), 3.13 (s, 3H, N-CH_3), 2.46 (s, 3H, pyrazolone ring -CH_3), 1.31 (s, 9H, *tert*-Bu).

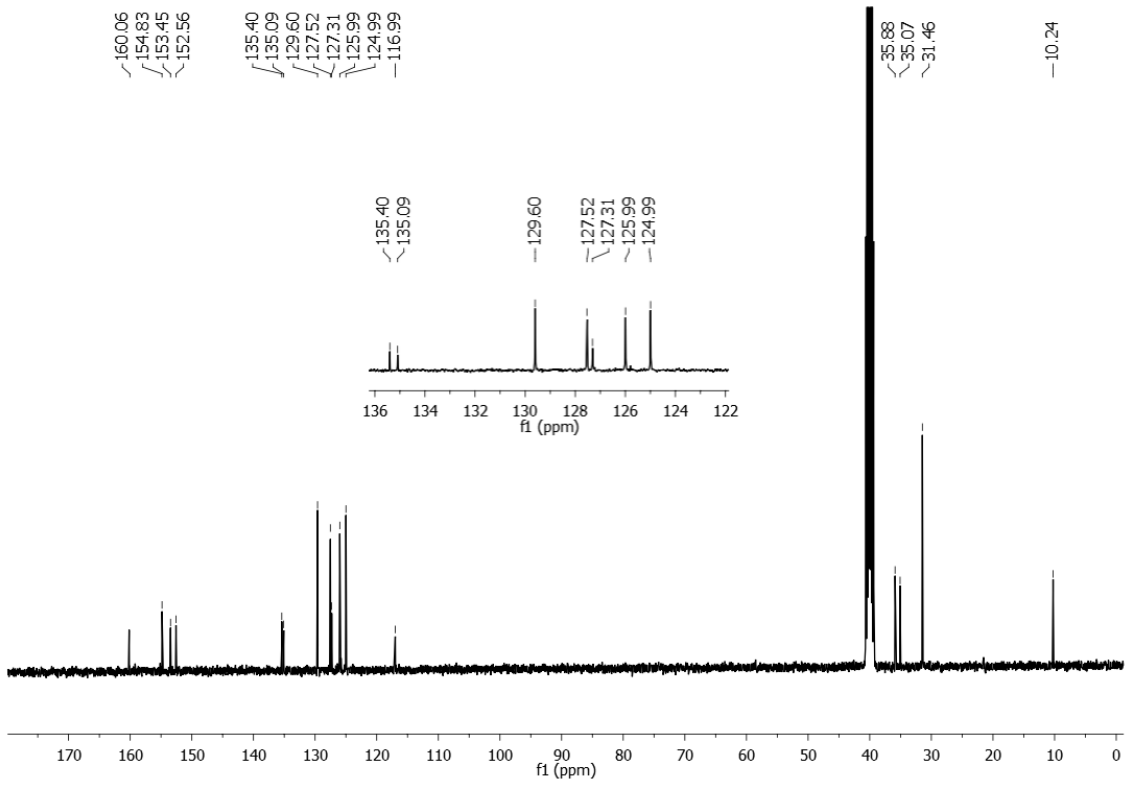

Figure 9. Experimental ^{13}C NMR spectra in DMSO-d_6 of the compound $C_{22}H_{25}N_3O$.

^{13}C NMR (DMSO-d_6, 100 MHz, δ ,ppm): 160.06 (-CH=N-), 154.83 (C=O), 153.45, 152.56, 135.40, 135.09, 129.60 (2C), 127.52 (2C), 127.31 (2C), 125.99 (2C), 124.99, 116.99, 35.88 (N-CH_3), 35.07 (*tert*-Bu C), 31.46 (*tert*-Bu CH_3), 10.24 (pyrazolone ring -CH_3).

4. Conclusion and Comment

In this study, we have investigated the molecular structure of $C_{22}H_{25}N_3O$, using single crystal X-ray diffraction, IR, NMR spectroscopy, and computational methods. The results obtained show that the X-ray crystal structure and computational methods are consistent with each other. There was particularly good agreement using the DFT (B3LYP) with the 6-31+G(d) basis set. The structural X-ray analysis has indicated that the crystal structure is the most stable structure with intermolecular C-H…π interactions. These results were consistent with those obtained by a MEP analysis. The calculated and observed C=O and C=N vibrations in the IR spectrum confirm the keto-imine tautomeric form of the structure. UV and NMR spectra were observed to be in harmony with the structure.

References

[1] P. Przybylski, A. Huczynski, K. Pyta, B. Brzezinski, and F. Bartl, "Biological Properties of Schiff Bases and Azo Derivatives of Phenols," *Curr. Org. Chem*., vol. 13, no. 2, pp. 124-148, Jan 2009.

[2] A. Osowole and E. Akpan, "Synthesis spectroscopic characterisation, in-vitro anticancer and antimicrobial activities of some metal (II) complexes of 3-{4, 6-dimethoxy pyrimidinyl) iminomethyl naphthalen-2-ol," *Eur. J. Appl. Sci*, vol. 4, pp. 14-20, 2012.

[3] M. Suresh and V. Prakash, "Preparation and characterization of Cr (III), Mn (II), Co (III), Ni (II), Cu (II), Zn (II) and Cd (II) chelates of schiffs base derived from vanillin and 4-amino antipyrine," *Int. J. Phys. Sci*., vol. 5, no. 14, pp. 2203-2211, 2010.

[4] Z. M. Bedeui, "Synthesis And Characterization Of Schiff-Base Ligand Derivative From 4-Aminoantipyrine And Its Transition Metal Complexes," *Journals kufa for chamical*, no. 8, pp. 70-78, 2013.

[5] A. K. Singh, G. Saxena, R. Prasad, and A. Kumar, "Synthesis, characterization and calculated non-linear optical properties of two new chalcones," *J. Mol. Struct.*, vol. 1017, pp. 26-31, 2012.
[6] L. Guo, S. Hong, X. Lin, Z. Xie, and G. Chen, "An organically modified sol–gel membrane for detection of lead ion by using 2-hydroxy-1-naphthaldehydene-8-aminoquinoline as fluorescence probe," *Sensor. Actuat. B-Chem.*, vol. 130, no. 2, pp. 789-794, 2008.
[7] N. Raman, J. D. Raja, and A. Sakthivel, "Synthesis, spectral characterization of Schiff base transition metal complexes: DNA cleavage and antimicrobial activity studies," *J. Chem. Sci.*, vol. 119, no. 4, pp. 303-310, 2007.
[8] M. S. Alam, D.-U. Lee, and M. L. Bari, "Antibacterial and cytotoxic activities of Schiff base analogues of 4-aminoantipyrine," *J. Korean Soc. Appl. Bi.*, vol. 57, no. 5, pp. 613-619, 2014.
[9] Stoe and X. Cie, "Area (Version 1.18) and X-Red32 (Version 1.04)," *Stoe&Cie, Darmstadt, Germany*, 2002.
[10] G. M. Sheldrick, "A short history of SHELX," *Acta. Crystallogr. Section. A.*, vol. 64, no. 1, pp. 112-122, 2008.
[11] G. M. Sheldrick, "Crystal structure refinement with SHELXL," *Acta. Crystallogr. C.*, vol. 71, no. 1, pp. 3-8, 2015.
[12] L. J. Farrugia, "WinGX and ORTEP for Windows: an update," *Journal of Applied Crystallography*, vol. 45, no. 4, pp. 849-854, 2012.
[13] M.J.Frisch, G.W.Trucks, H.B. Schlegel, G.E.Scuseria, M. A. Robb, J. R. Cheeseman, et al. "Gaussian 03, Revision E. 01. Gaussian Inc.", Wallingford CT 2004.
[14] A. Frisch, R. II Dennington, T. Keith, J. Millam, A.B. Nielsen, A.J. Holder, et al. "GaussView reference, version 4.0. Gaussian Inc.", Pittsburgh. 2007.
[15] C. Lee, W. Yang, and R. G. Parr, "Development of the Colle-Salvetti correlation-energy formula into a functional of the electron density," *Phys. Rev. B.*, vol. 37, no. 2, p. 785, 1988.
[16] A. Becke, "Density-functional thermochemistry. III. The role of exact exchange," *J. Chem. Phys.*, vol. 98, no. 7, p. 5648, 1993.
[17] P. Politzer, J. S. Murray, and M. C. Concha, "The complementary roles of molecular surface electrostatic potentials and average local ionization energies with respect to electrophilic processes," *International Journal of Quantum Chemistry*, vol. 88, no. 1, pp. 19-27, 2002.
[18] N. Okulik and A. H. Jubert, "Theoretical analysis of the reactive sites of non-steroidal anti-inflammatory drugs," *Internet Electronic Journal of Molecular Design*, vol. 4, no. 1, pp. 17-30, 2005.
[19] F. J. Luque, J. M. López, and M. Orozco, "Perspective on "Electrostatic interactions of a solute with a continuum. A direct utilization of ab initio molecular potentials for the prevision of solvent effects"," *Theor. Chem. Acc.*, vol. 103, no. 3-4, pp. 343-345, 2000.
[20] E. Scrocco and J. Tomasi, "Electronic molecular structure, reactivity and intermolecular forces: an euristic interpretation by means of electrostatic molecular potentials," in *Advances in quantum chemistry*, vol. 11: Elsevier, 1978, pp. 115-193.
[21] G. Socrates, "Infrared Characteristic Group Frequencies, J," *John Wily & Sons, NY*, p. 115, 1980.
[22] H. Bülbül, Y. Köysal, N. Dege, S. Gümüş, and E. Ağar, "Crystal structure, spectroscopy, SEM analysis, and computational studies of N-(1, 3-Dioxoisoindolin-2yl) benzamide," *Journal of Crystallography*, vol. 2015, Artcile id 232036 (6 p.), 2015.
[23] M. Evecen, H. Tanak, Y. Ünver, F. Çelik, and L. Semiz, "Analysis on molecular, spectroscopic and electronic behavior of 4, 4'-(butane-1, 4-diyl) bis (1-((1-(4-chlorobenzyl)-1H-1, 2, 3-triazol-5-yl) methyl)-3-methyl-1H-1, 2, 4-triazol-5 (4H)-one): A theoretical approach," *J. Mol. Struct.*, vol. 1174, pp. 60-66, 2018.

Şehriman ATALAY, atalays@omu.edu.tr, ORCID: https://orcid.org/0000-0002-4175-3477